Rock Mech. Rock Engng. (2004) 37 (2), 95–116
DOI 10.1007/s00603-003-0008-x

Rock Mechanics and Rock Engineering
Printed in Austria

A Model of Point-to-Face Contact for Three-Dimensional Discontinuous Deformation Analysis

By

Q. H. Jiang[1] and **M. R. Yeung**[2]

[1]State Key Laboratory of Water Resources and Hydropower Engineering Science
Wuhan University, Wuhan, P.R. China
[2]Department of Civil Engineering, The University of Hong Kong,
Hong Kong, P.R. China

Received August 30, 2002; accepted April 7, 2003
Published online August 18, 2003

Summary

The key to three-dimensional discontinuous deformation analysis (3D DDA) is a rigorous contact theory that governs the interaction of many three-dimensional blocks. This theory must provide algorithms to judge contact types and locations and the appropriate state of each contact, which can be open, sliding or locked. This paper presents a point-to-face contact model, which forms a part of the contact theory, to be used in 3D DDA. Normal spring, shear spring and frictional force submatrices are derived by vector analysis and the penalty method. Also given are the "open-close" iteration criteria and operations performed for different changes in contact state. Sliding at a contact can occur in any direction parallel to the contact face, as opposed to one of two directions in two-dimensional DDA. This point-to-face contact model has been implemented into a 3D DDA computer program, and numerical results from several test cases demonstrate the validity of the model and the capability of the program.

Keywords: 3D DDA, point-to-face contact, open-close iteration.

1. Introduction

The discontinuous deformation analysis (DDA) is a numerical model for block systems that can be used to analyse jointed rock mass behaviour (Shi, 1988; Shi and Goodman, 1989). Using DDA, one can perform static and dynamic analysis of a block system to obtain solutions of large deformation and large displacement. The DDA model introduces a unified format for the consideration of not only the displacement, rotation and deformation of an individual rock block but also such movement forms as sliding and opening along block boundaries, having the advantages of both the distinct

element method (DEM) and the finite element method (FEM). DDA has received considerable attention from researchers and practising engineers and has become a useful tool for the analysis of jointed rock mass behaviour.

The original DDA is a two-dimensional (2D) numerical model, and significant recent development of DDA has been focused on extending the capabilities of the 2D model (Yeung, 1993; Lin et al., 1996; Chern et al., 1990; Thomas and Bray, 1999; Koo and Chern, 1998; Chen et al., 1997; Kim et al., 1999; Ke, 1996; Hatzor and Feintuch, 2001; Jing et al., 2001; Sitar and MacLaughlin, 1997). There is an obvious need for a 3D model because of the highly directional nature of jointed rock mass behaviour, making the application of 2D DDA to many practical problems inappropriate. While various researchers are working on three-dimensional discontinuous deformation analysis (3D DDA), only preliminary work on this subject has been published without a complete contact theory that governs the interaction of many 3D blocks (Shi, 2001).

In the contact theory for 3D DDA, the first step is to determine the type of contact between any two arbitrarily shaped polyhedral blocks. The type of contact is important because it determines the mechanical response of the contact. There are many more types of contacts for 3D blocks than for 2D ones. In two dimensions, the contact types include corner-to-corner, corner-to-edge and edge-to-edge; whereas 3D contact types include vertex-to-vertex, vertex-to-edge, vertex-to-face, edge-to-edge, edge-to-face and face-to-face. In the contact theory of which the point-to-face contact model presented in this paper is a part, the common-plane method of Cundall (1988) is used to determine the contact type. Using this method, contacts may be classified into different types by determining how many vertices of each block touch the common-plane. Once the contact types and contact faces are determined, all contacts can be converted to one or more point-to-face contacts, as shown for example in Fig. 1, similar to what is done in 2D DDA in which all contacts can be converted to corner-to-edge contacts. The generic contact type in 3D is called point-to-face and not vertex-to-face because, as can be seen in Fig. 1, a converted contact can be between a point on an edge and a face.

The contact problem is highly non-linear in nature. Although studies have been carried out on the frictional contact problem for several decades, it is still one of the

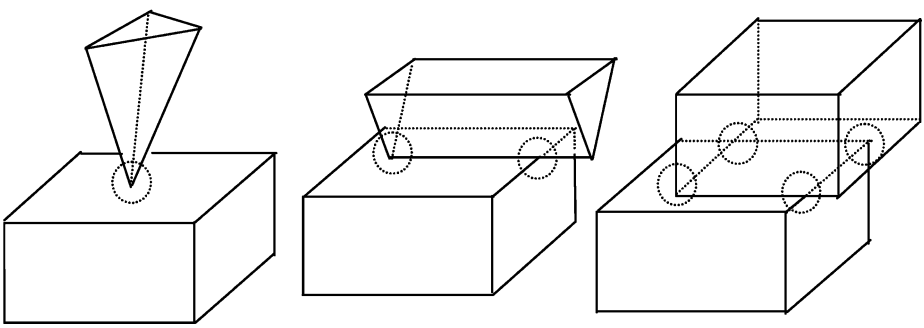

Fig. 1. ◌ Point-to-face contacts

most difficult problems to handle. Especially in the 3D case, the relative sliding of the contact point may occur in any direction parallel to the contact face, as opposed to one of two directions in the 2D case; hence, more complicated block interaction problems will be encountered. Moreover, non-convergence is more likely to occur in the 3D case than in the 2D case. Numerical analysis techniques for solving frictional contact problems are established using the trial-and-error iterative method (Francavilla and Zienkiewicz, 1975; Rahman et al., 1984; Hong et al., 1998), the penalty method (Oden and Kikuchi, 1982; Kanto and Yagawa, 1990; Yamazaki et al., 1994; Munjiza and Andrews, 2000), the Lagrangian multiplier method (Chen and Tsai, 1986; Chaudhary and Bathe, 1986; Bathe and Chaudhary, 1985), the mathematical programming method (Klarbring, 1986; Fischer and Melosh, 1987), and other methods (Leung et al., 1998; Li et al., 2000). Among these methods, the penalty method is one of the most efficient because this method does not require an increase in the number of degrees of freedom in the final equation to be solved.

This paper presents a model of point-to-face contact to be used in 3D DDA. Contact submatrices, including those for the normal spring, shear spring and the frictional forces, are derived by vector analysis and the penalty method. This point-to-face contact model has been implemented into a 3D DDA computer program, and numerical results from several test cases demonstrate the validity of the model and the capability of the program.

2. Basic Principles of DDA

2.1 Displacement and Deformation of a 3D Block

DDA uses time steps for both statics and dynamics. The large deformation in a block and the large relative movements between blocks are accumulated over many time steps. Given that for each time step, the condition of small displacement and deformation is satisfied and assuming that a 3D arbitrarily shaped polyhedral block has uniform stress and strain, the movement and the deformation of the block are defined by 12 independent kinematic variables in the displacement matrix $[D_i]$:

$$\begin{aligned}[D_i] &= [d_1, d_2, d_3, d_4, d_5, d_6, d_7, d_8, d_9, d_{10}, d_{11}, d_{12}]^T \\ &= [u_0, v_0, w_0, \alpha_0, \beta_0, \gamma_0, \varepsilon_x, \varepsilon_y, \varepsilon_z, \gamma_{xy}, \gamma_{yz}, \gamma_{zx}]^T, \end{aligned} \tag{1}$$

where (u_0, v_0, w_0) are the x-, y- and z-translations, respectively, of the block's centre of mass (x_0, y_0, z_0); $(\alpha_0, \beta_0, \gamma_0)$ are the rotations of the block about the x-, y- and z-axes, respectively; and $(\varepsilon_x, \varepsilon_y, \varepsilon_z, \gamma_{xy}, \gamma_{yz}, \gamma_{zx})$ are the three normal strains and three shear strains of the block.

The x-, y- and z-displacements (u, v, w) of an arbitrary point (x, y, z) in the block can be expressed in terms of the kinematic variables of $[D_i]$:

$$\begin{bmatrix} u \\ v \\ w \end{bmatrix} = [T_i]\ [D_i] = \begin{bmatrix} \sum_{j=1}^{12} t_{1j} d_j \\ \sum_{j=1}^{12} t_{2j} d_j \\ \sum_{j=1}^{12} t_{3j} d_j \end{bmatrix}, \tag{2}$$

where

$$[T_i] = \begin{bmatrix} 1 & 0 & 0 & 0 & (z-z_0) & -(y-y_0) & (x-x_0) & 0 & 0 & (y-y_0)/2 & 0 & (z-z_0)/2 \\ 0 & 1 & 0 & -(z-z_0) & 0 & (x-x_0) & 0 & (y-y_0) & 0 & (x-x_0)/2 & (z-z_0)/2 & 0 \\ 0 & 0 & 1 & (y-y_0) & -(x-x_0) & 0 & 0 & 0 & (z-z_0) & 0 & (y-y_0)/2 & (x-x_0)/2 \end{bmatrix}. \tag{3}$$

$[T_i]$ is called the displacement transformation matrix of the block.

Error due to approximation using a linear displacement function causes block expansion, especially in problems involving large rigid body rotations (Koo and Chern, 1998; Ke, 1996). To correct the error, post-correction is used and the *x*-, *y*- and *z*-displacements (*u, v, w*) of all relevant points including block vertices are recalculated using Eq. (4) after each time step:

$$\begin{bmatrix} u \\ v \\ w \end{bmatrix} = \begin{bmatrix} \sum_{j=1}^{12} t_{1j} d_j \\ \sum_{j=1}^{12} t_{2j} d_j \\ \sum_{j=1}^{12} t_{3j} d_j \end{bmatrix}_{j \neq 4,5,6} + \begin{bmatrix} \cos\beta_0 + \cos\gamma_0 - 2 & -\sin\gamma_0 & \sin\beta_0 \\ \sin\gamma_0 & \cos\alpha_0 + \cos\gamma_0 - 2 & -\sin\alpha_0 \\ -\sin\beta_0 & \sin\alpha_0 & \cos\alpha_0 + \cos\beta_0 - 2 \end{bmatrix} \begin{bmatrix} x - x_0 \\ y - y_0 \\ z - z_0 \end{bmatrix}. \tag{4}$$

2.2 General Equilibrium Equations

A number of individual blocks can be connected to form a block system satisfying the constraints between blocks. For a system of n blocks, its behaviour is governed by the following system of simultaneous equations:

$$\begin{bmatrix} K_{11} & K_{12} & K_{13} & \cdots & K_{1n} \\ K_{21} & K_{22} & K_{23} & \cdots & K_{2n} \\ K_{31} & K_{32} & K_{33} & \cdots & K_{3n} \\ \vdots & \vdots & \vdots & \ddots & \vdots \\ K_{n1} & K_{n2} & K_{n3} & \cdots & K_{nn} \end{bmatrix} \begin{bmatrix} D_1 \\ D_2 \\ D_3 \\ \vdots \\ D_n \end{bmatrix} = \begin{bmatrix} F_1 \\ F_2 \\ F_3 \\ \vdots \\ F_n \end{bmatrix}. \tag{5}$$

Each 3D block has 12 degrees of freedom, so in the coefficient matrix of Eq. (5), each element $[K_{ij}]$ is a 12×12 submatrix. $[D_i]$ and $[F_i]$ are 12×1 submatrices, with $[D_i]$ containing the kinematic variables of block i and $[F_i]$ containing the loads on block i distributed to the 12 kinematic variables. The submatrix $[K_{ii}]$ depends on the material properties of block i, and $[K_{ij}]$ $(i \neq j)$ is determined by the contact condition between block i and block j. Eq. (5) can also be expressed in a more compact form of $[K][D] = [F]$, where $[K]$ is a $12n \times 12n$ stiffness matrix, and $[D]$ and $[F]$ are $12n \times 1$ displacement and force matrices, respectively. In total, the number of displacement unknowns is the sum of the degrees of freedom of all the blocks.

Equation (5) was derived by Shi (2001) by minimizing the total potential energy Π of the block system. The i-th row of Eq. (5) consists of 12 linear equations

$$\frac{\partial \Pi}{\partial d_{ri}} = 0, \quad r = 1-12, \tag{6}$$

where $d_{ri} (r = 1-12)$ are the kinematic variables of block i. The total potential energy is the sum from all potential energy sources, i.e. individual stresses and forces. The potential energy of each force or stress and its derivative are considered

separately. The derivative

$$\frac{\partial^2 \Pi}{\partial d_{ri} \partial d_{sj}}, \quad r, s = 1-12 \tag{7}$$

is the coefficient of unknown d_{sj} in Eq. (6) for variable d_{ri}. All terms of Eq. (7) form a 12×12 submatrix, which is added to the submatrix $[K_{ij}]$ in Eq. (5). Eq. (7) implies that the global stiffness matrix $[K]$ is symmetric. The derivative

$$-\frac{\partial \Pi(0)}{\partial d_{ri}}, \quad r = 1-12 \tag{8}$$

is the free term of Eq. (6) which is shifted to the right hand side of Eq. (5). All terms of Eq. (8) form a 12×1 submatrix, which is added to the submatrix $[F_i]$ in Eq. (5).

3. Point-to-Face Contact Model

3.1 Normal Spring Submatrices

For the point-to-face contact between two arbitrarily shaped polyhedral blocks shown in Fig. 2, the point in question is $P_1(x_1, y_1, z_1)$, which is a vertex of block i, and the polygon $P_2P_3 \cdots P_6$ is the contact face, which is a face of block j. $P_0(x_0, y_0, z_0)$ is the projection of point $P_1(x_1, y_1, z_1)$ on the face $P_2P_3 \cdots P_6$. Let (x_i, y_i, z_i) and (u_i, v_i, w_i) be the coordinates and displacement increments, respectively, of the vertices $P_i(i = 0-6)$, and let $P_i'(i = 0-6)$ be the respective vertices after the displacement

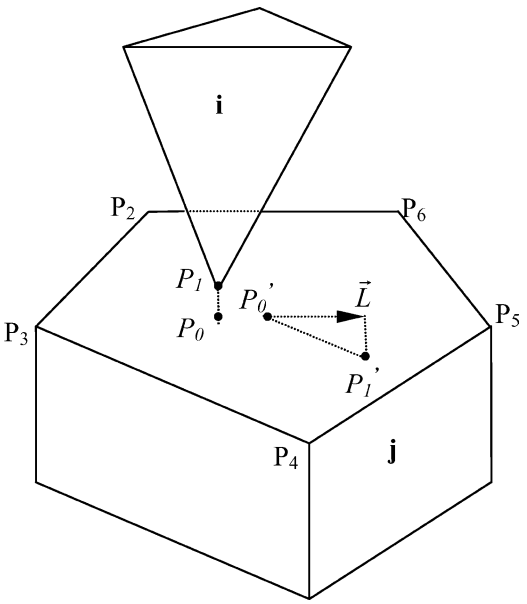

Fig. 2. Point-to-face contact

increments are applied. After the displacement increments are applied, the vector pointing out of the block that is normal to the contact face $P_2'P_3'\cdots P_6'$ is given by

$$\begin{aligned}\overrightarrow{n} &= \overrightarrow{P_2'P_3'} \times \overrightarrow{P_2'P_4'} \\ &= \begin{vmatrix} \vec{i} & \vec{j} & \vec{k} \\ x_3+u_3-x_2-u_2 & y_3+v_3-y_2-v_2 & z_3+w_3-z_2-w_2 \\ x_4+u_4-x_2-u_2 & y_4+v_4-y_2-v_2 & z_4+w_4-z_2-w_2 \end{vmatrix}. \end{aligned} \tag{9}$$

Therefore,

$$\overrightarrow{n} = [(e_{11}+e_{12}+e_{13}+e_{14})(e_{21}+e_{22}+e_{23}+e_{24})(e_{31}+e_{32}+e_{33}+e_{34})], \tag{10}$$

where

$$\begin{aligned} e_{11} &= \begin{vmatrix} y_3-y_2 & z_3-z_2 \\ y_4-y_2 & z_4-z_2 \end{vmatrix} \quad e_{12} = \begin{vmatrix} y_3-y_2 & w_3-w_2 \\ y_4-y_2 & w_4-w_2 \end{vmatrix} \quad e_{13} = \begin{vmatrix} v_3-v_2 & z_3-z_2 \\ v_4-v_2 & z_4-z_2 \end{vmatrix} \\ e_{14} &= \begin{vmatrix} v_3-v_2 & w_3-w_2 \\ v_4-v_2 & w_4-w_2 \end{vmatrix} \quad e_{21} = \begin{vmatrix} z_3-z_2 & x_3-x_2 \\ z_4-z_2 & x_4-x_2 \end{vmatrix} \quad e_{22} = \begin{vmatrix} z_3-z_2 & u_3-u_2 \\ z_4-z_2 & u_4-u_2 \end{vmatrix} \\ e_{23} &= \begin{vmatrix} w_3-w_2 & x_3-x_2 \\ w_4-w_2 & x_4-x_2 \end{vmatrix} \quad e_{24} = \begin{vmatrix} w_3-w_2 & u_3-u_2 \\ w_4-w_2 & u_4-u_2 \end{vmatrix} \quad e_{31} = \begin{vmatrix} x_3-x_2 & y_3-y_2 \\ x_4-x_2 & y_4-y_2 \end{vmatrix} \\ e_{32} &= \begin{vmatrix} x_3-x_2 & v_3-v_2 \\ x_4-x_2 & v_4-v_2 \end{vmatrix} \quad e_{33} = \begin{vmatrix} u_3-u_2 & y_3-y_2 \\ u_4-u_2 & y_4-y_2 \end{vmatrix} \quad e_{34} = \begin{vmatrix} u_3-u_2 & v_3-v_2 \\ u_4-u_2 & v_4-v_2 \end{vmatrix}. \end{aligned}$$

The normal distance between the point P_1' and the contact face $P_2'P_3'\ldots P_6'$, d_n, is given by

$$d_n = \frac{\Delta}{l} = \frac{1}{l}\overrightarrow{n}\cdot\overrightarrow{P_0'P_1'}, \tag{11}$$

where l is the length of the normal vector $\vec{n}$ and Δ is given by

$$\begin{aligned} \Delta = {} & [e_{11} \quad e_{21} \quad e_{31}] \begin{bmatrix} (x_1-x_0)+(u_1-u_0) \\ (y_1-y_0)+(v_1-v_0) \\ (z_1-z_0)+(w_1-w_0) \end{bmatrix} \\ & + [e_{12} \quad e_{22} \quad e_{32}] \begin{bmatrix} (x_1-x_0)+(u_1-u_0) \\ (y_1-y_0)+(v_1-v_0) \\ (z_1-z_0)+(w_1-w_0) \end{bmatrix} \\ & + [e_{13} \quad e_{23} \quad e_{33}] \begin{bmatrix} (x_1-x_0)+(u_1-u_0) \\ (y_1-y_0)+(v_1-v_0) \\ (z_1-z_0)+(w_1-w_0) \end{bmatrix} \\ & + [e_{14} \quad e_{24} \quad e_{34}] \begin{bmatrix} (x_1-x_0)+(u_1-u_0) \\ (y_1-y_0)+(v_1-v_0) \\ (z_1-z_0)+(w_1-w_0) \end{bmatrix}. \end{aligned} \tag{12}$$

The step displacement increments (u_i, v_i, w_i), $i = 0$–6, are small for small time steps. The contact distance P_0P_1 is small from the definition of a contact. Therefore, expanding the right side of Eq. (12), the first term gives first order infinitesimal terms; the second and third terms give second order infinitesimal terms; and the last term gives third order infinitesimal terms.

Let

$$S_0 = [e_{11} \quad e_{21} \quad e_{31}] \begin{bmatrix} x_1 - x_0 \\ y_1 - y_0 \\ z_1 - z_0 \end{bmatrix} \tag{13}$$

Neglecting the second and third order infinitesimal terms, Eq. (12) can then be approximated as

$$\Delta \approx S_0 + [e_{11} \quad e_{21} \quad e_{31}] \begin{bmatrix} u_1 \\ v_1 \\ w_1 \end{bmatrix} + [-e_{11} \quad -e_{21} \quad -e_{31}] \begin{bmatrix} u_0 \\ v_0 \\ w_0 \end{bmatrix}. \tag{14}$$

Also, the expression for l can then be simplified as

$$l = \sqrt{e_{11}^2 + e_{21}^2 + e_{31}^2}. \tag{15}$$

From Eqs. (2), (11) and (14),

$$d_n = \frac{S_0}{l} + [E_i][D_i] + [G_j][D_j], \tag{16}$$

where $[E_i]$ and $[G_j]$ are 1×12 matrices with components e_r and g_r ($r = 1$–12) given by

$$\begin{aligned} e_r &= \frac{1}{l}\left[e_{11}t_{1r}^i(x_1, y_1, z_1) + e_{21}t_{2r}^i(x_1, y_1, z_1) + e_{31}t_{3r}^i(x_1, y_1, z_1)\right], \\ g_r &= \frac{-1}{l}\left[e_{11}t_{1r}^j(x_0, y_0, z_0) + e_{21}t_{2r}^j(x_0, y_0, z_0) + e_{31}t_{3r}^j(x_0, y_0, z_0)\right], \end{aligned} \tag{17}$$

where t_{1r}, t_{2r} and t_{3r} are the components of matrix $[T_i]$ in Eq. (3).

Using the penalty method, a mathematical spring is placed between point P_1 and the contact face $P_2P_3 \cdots P_6$ in the direction normal to the contact face. Denoting the stiffness of the spring as p_n, the potential energy of the normal spring is given by

$$\Pi_n = \frac{p_n}{2} {d_n}^2 = \frac{p_n}{2}\left(\frac{S_0}{l} + [E_i][D_i] + [G_j][D_j]\right)^2. \tag{18}$$

In general, p_n should be a large positive penalty number. This is to ensure the deformation of the spring is much smaller than that of the block. If the value of p_n is large enough, the computational results practically will not depend on the value of p_n.

Expanding the right side of Eq. (18) and minimising Π_n by taking derivatives, four 12×12 submatrices and two 12×1 submatrices are obtained and added to the submatrices $[K_{ii}]$, $[K_{ij}]$, $[K_{ji}]$, $[K_{jj}]$, $[F_i]$ and $[F_j]$, respectively, in the global equilibrium equation (Eq. (5)).

The derivatives of Π_n

$$k_{rs} = \frac{\partial^2 \Pi_n}{\partial d_{ri} \partial d_{si}} \quad r, s = 1-12$$
$$= \frac{p_n}{2} \frac{\partial^2}{\partial d_{ri} \partial d_{si}} [D_i]^T [E_i]^T [E_i] [D_i] \tag{19}$$

form a 12×12 submatrix which is added to the submatrix $[K_{ii}]$ in Eq. (5):

$$p_n [E_i]^T [E_i] \rightarrow [K_{ii}]. \tag{20}$$

The derivatives of Π_n

$$k_{rs} = \frac{\partial^2 \Pi_n}{\partial d_{ri} \partial d_{sj}} \quad r, s = 1-12$$
$$= p_n \frac{\partial^2}{\partial d_{ri} \partial d_{sj}} [D_i]^T [E_i]^T [G_j] [D_j] \tag{21}$$

form a 12×12 submatrix which is added to the submatrix $[K_{ij}]$ in Eq. (5):

$$p_n [E_i]^T [G_j] \rightarrow [K_{ij}]. \tag{22}$$

The derivatives of Π_n

$$k_{rs} = \frac{\partial^2 \Pi_n}{\partial d_{rj} \partial d_{si}} \quad r, s = 1-12$$
$$= p_n \frac{\partial^2}{\partial d_{rj} \partial d_{si}} [D_j]^T [G_j]^T [E_i] [D_i] \tag{23}$$

form a 12×12 submatrix which is added to the submatrix $[K_{ji}]$ in Eq. (5):

$$p_n [G_j]^T [E_i] \rightarrow [K_{ji}]. \tag{24}$$

The derivatives of Π_n

$$k_{rs} = \frac{\partial^2 \Pi_n}{\partial d_{rj} \partial d_{sj}} \quad r, s = 1-12$$
$$= \frac{p_n}{2} \frac{\partial^2}{\partial d_{rj} \partial d_{sj}} [D_j]^T [G_j]^T [G_j] [D_j] \tag{25}$$

form a 12×12 submatrix which is added to the submatrix $[K_{jj}]$ in Eq. (5):

$$p_n [G_j]^T [G_j] \rightarrow [K_{jj}]. \tag{26}$$

The derivatives of Π_n at 0

$$f_{ri} = -\frac{\partial \Pi_n(0)}{\partial d_{ri}} \quad r = 1-12 \tag{27}$$

form a 12×1 submatrix which is added to the submatrix $[F_i]$ in Eq. (5):

$$-\frac{p_n S_0}{l}[E_i]^T \rightarrow [F_i]. \tag{28}$$

The derivatives of Π_n at 0

$$f_{rj} = -\frac{\partial \Pi_n(0)}{\partial d_{rj}} \quad r = 1-12 \tag{29}$$

form a 12×1 submatrix which is added to the submatrix $[F_j]$ in Eq. (5):

$$-\frac{p_n S_0}{l}[G_j]^T \rightarrow [F_j]. \tag{30}$$

3.2 Shear Spring Submatrices

As shown in Fig. 2, points P_1 and P_0 move to P_1' and P_0', respectively, after the displacement increments are applied. Let $\vec{L}$ be the projection of the vector $\overrightarrow{P_0'P_1'}$ on the contact face $P_2'P_3' \cdots P_6'$. The magnitude of $\vec{L}$ is given by

$$|\vec{L}| = d_s = \sqrt{|\overrightarrow{P_0'P_1'}|^2 - {d_n}^2}. \tag{31}$$

Assuming there is a shear spring between points P_1 and P_0 in a direction parallel to $\vec{L}$ and letting p_s be the stiffness of the shear spring, the potential energy of the shear spring is given by

$$\begin{aligned}\Pi_s &= \frac{p_s}{2}{d_s}^2 = \frac{p_s}{2}(|\overrightarrow{P_1'P_0'}|^2 - {d_n}^2) \\ &= \frac{p_s}{2}[\,x_1 + u_1 - x_0 - u_0 \quad y_1 + v_1 - y_0 - v_0 \quad z_1 + w_1 - z_0 - w_0\,] \\ &\quad \cdot \begin{bmatrix} x_1 + u_1 - x_0 - u_0 \\ y_1 + v_1 - y_0 - v_0 \\ z_1 + w_1 - z_0 - w_0 \end{bmatrix} - \frac{p_s}{2} d_n^2. \end{aligned} \tag{32}$$

From Eqs. (2), (18) and (32),

$$\begin{aligned}\Pi_s = \frac{p_s}{2}&([\,x_1 - x_0 \quad y_1 - y_0 \quad z_1 - z_0\,] + [D_i]^T[T_i]^T - [D_j]^T[T_j]^T) \\ &\cdot \left(\begin{bmatrix} x_1 - x_0 \\ y_1 - y_0 \\ z_1 - z_0 \end{bmatrix} + [T_i][D_i] - [T_j][D_j] \right) - \frac{p_s}{2}\left(\frac{S_0}{l} + [E_i][D_i] + [G_j][D_j] \right)^2. \end{aligned} \tag{33}$$

In general, p_s should be a large positive penalty number. If the value of p_s is large enough, the computational results practically will not depend on the value of p_s.

Expanding the right side of Eq. (33) and minimising Π_s by taking derivatives, four 12×12 submatrices and two 12×1 submatrices are obtained and added to the

submatrices $[K_{ii}]$, $[K_{ij}]$, $[K_{ji}]$, $[K_{jj}]$, $[F_i]$ and $[F_j]$, respectively, in the global equilibrium equation (Eq. (5)).

The derivatives of Π_s

$$k_{rs} = \frac{\partial^2 \Pi_s}{\partial d_{ri} \partial d_{si}} \quad r, s = 1-12$$
$$= \frac{p_s}{2} \frac{\partial^2}{\partial d_{ri} \partial d_{si}} ([D_i]^T [T_i]^T [T_i][D_i] - [D_i]^T [E_i]^T [E_i][D_i]) \tag{34}$$

form a 12×12 submatrix which is added to the submatrix $[K_{ii}]$ in Eq. (5):

$$p_s [T_i]^T [T_i] - p_s [E_i]^T [E_i] \rightarrow [K_{ii}]. \tag{35}$$

The derivatives of Π_s

$$k_{rs} = \frac{\partial^2 \Pi_s}{\partial d_{ri} \partial d_{sj}} \quad r, s = 1-12$$
$$= p_s \frac{\partial^2}{\partial d_{ri} \partial d_{sj}} (-[D_i]^T [T_i]^T [T_j][D_j] - [D_i]^T [E_i]^T [G_j][D_j]) \tag{36}$$

form a 12×12 submatrix which is added to the submatrix $[K_{ij}]$ in Eq. (5):

$$-p_s [T_i]^T [T_j] - p_s [E_i]^T [G_j] \rightarrow [K_{ij}]. \tag{37}$$

The derivatives of Π_s

$$k_{rs} = \frac{\partial^2 \Pi_s}{\partial d_{rj} \partial d_{si}} \quad r, s = 1-12$$
$$= p_s \frac{\partial^2}{\partial d_{rj} \partial d_{si}} (-[D_j]^T [T_j]^T [T_i][D_i] - [D_j]^T [G_j]^T [E_i][D_i]) \tag{38}$$

form a 12×12 submatrix which is added to the submatrix $[K_{ji}]$ in Eq. (5):

$$-p_s [T_j]^T [T_i] - p_s [G_j]^T [E_i] \rightarrow [K_{ji}]. \tag{39}$$

The derivatives of Π_s

$$k_{rs} = \frac{\partial^2 \Pi_s}{\partial d_{rj} \partial d_{sj}} \quad r, s = 1-12$$
$$= \frac{p_s}{2} \frac{\partial^2}{\partial d_{rj} \partial d_{sj}} ([D_j]^T [T_j]^T [T_j][D_j] - [D_j]^T [G_j]^T [G_j][D_j]) \tag{40}$$

form a 12×12 submatrix which is added to the submatrix $[K_{jj}]$ in Eq. (5):

$$p_s [T_j]^T [T_j] - p_s [G_j]^T [G_j] \rightarrow [K_{jj}]. \tag{41}$$

The derivatives of Π_s at 0

$$f_{ri} = -\frac{\partial \Pi_s(0)}{\partial d_{ri}} \quad r = 1-12 \tag{42}$$

form a 12×1 submatrix which is added to the submatrix $[F_i]$ in Eq. (5):

$$-p_s[T_i]^T \begin{bmatrix} x_1 - x_0 \\ y_1 - y_0 \\ z_1 - z_0 \end{bmatrix} + \frac{p_s S_0}{l}[E_i]^T \rightarrow [F_i]. \tag{43}$$

The derivatives of Π_s at 0

$$f_{rj} = -\frac{\partial \Pi_s(0)}{\partial d_{rj}} \quad r = 1-12 \tag{44}$$

form a 12×1 submatrix which is added to the submatrix $[F_j]$ in Eq. (5):

$$p_s[T_j]^T \begin{bmatrix} x_1 - x_0 \\ y_1 - y_0 \\ z_1 - z_0 \end{bmatrix} + \frac{p_s S_0}{l}[G_j]^T \rightarrow [F_j]. \tag{45}$$

3.3 Frictional Force Submatrices

For the 3D contact problem, sliding at the contact point may occur in any direction parallel to the contact face. We propose an iterative procedure for determining the frictional force and the sliding direction. For the point-to-face contact shown in Fig. 2, the point, or vertex, P_1 is on block i and its projection P_0 is on block j. When the state of the point-to-face contact is sliding, a pair of equal and opposite frictional forces parallel to the sliding direction is applied, one at the point P_1 and one at the point P_0 on the face. The magnitude and directions of the frictional forces are obtained from the previous iteration. The frictional force magnitude F is calculated from the normal contact compressive force from the previous iteration:

$$F = p_n |d_n'| \tan \phi \tag{46}$$

where p_n is the normal spring stiffness; d_n' is the normal penetration distance after the previous iteration; and ϕ is the friction angle.

Let ${P_0}^*$ and ${P_1}^*$ be the vertices P_0 and P_1, respectively, after the previous iteration. The direction of the frictional force acting at P_0 is assumed to be in the direction of $\vec{L}_1$, which is the projection of the vector $\overrightarrow{{P_0}^*{P_1}^*}$ on the undeformed contact face $P_2P_3 \cdots P_6$, and the direction of the frictional force acting at P_1 is assumed to be opposite to that of $\vec{L}_1$. Now, let $\overrightarrow{n'}$ be the unit vector pointing out of the block that is normal to the undeformed contact face $P_2P_3 \cdots P_6$ and (u_i', v_i', w_i'), $i = 0-1$, be the displacement increments of points $P_i (i = 0-1)$, respectively, from the previous iteration. Then

$$\overrightarrow{{P_0}^*{P_1}^*} = [\,(x_1 + {u_1}' - x_0 - {u_0}') \quad (y_1 + {v_1}' - y_0 - {v_0}') \quad (z_1 + {w_1}' - z_0 - {w_0}')] \tag{47}$$

and

$$\overrightarrow{n'} = \frac{1}{l}[\,e_{11} \quad e_{21} \quad e_{31}\,]. \tag{48}$$

Therefore,

$$\vec{L}_1 = [\,d \quad e \quad f\,] = \overrightarrow{{P_0}^*{P_1}^*} - (\overrightarrow{{P_0}^*{P_1}^*} \cdot \overrightarrow{n'})\overrightarrow{n'} \tag{49}$$

Then, the potential energy of the pair of frictional forces is given by

$$\begin{aligned}\Pi_f &= \frac{F}{|\vec{L}_1|}[\,u_1 - u_0 \quad v_1 - v_0 \quad w_1 - w_0\,][\,d \quad e \quad f\,]^T \\ &= F([D_i]^T[M] - [D_j]^T[N]),\end{aligned} \tag{50}$$

where

$$[M] = \frac{1}{|\vec{L}_1|}[T_i(x_1, y_1, z_1)]^T[\,d \quad e \quad f\,]^T,$$

and

$$[N] = \frac{1}{|\vec{L}_1|}[T_j(x_0, y_0, z_0)]^T[\,d \quad e \quad f\,]^T.$$

The relevant derivatives of Π_f with respect to d_{ri} and d_{rj} at 0

$$f_{ri} = -\frac{\partial \Pi_f(0)}{\partial d_{ri}} = -F\frac{\partial}{\partial d_{ri}}[D_i]^T[M] \quad r = 1-12 \tag{51}$$

and

$$f_{rj} = -\frac{\partial \Pi_f(0)}{\partial d_{rj}} = F\frac{\partial}{\partial d_{rj}}[D_j]^T[N] \qquad r = 1-12 \tag{52}$$

form two 12×1 submatrices which are added to the submatrices $[F_i]$ and $[F_j]$, respectively, in the global equilibrium equation (Eq. (5)):

$$-F[M] \rightarrow [F_i] \quad \text{and} \quad F[N] \rightarrow [F_j]. \tag{53}$$

After an iteration, the frictional force magnitude and directions are updated according to the results of the iteration.

3.4 "Open-Close" Iteration

Within each time step, the global system of equilibrium equations (Eq. (5)) are solved repeatedly while selecting the types, locations and states of contacts. The procedure of adding and removing stiff springs depending on the changes in contact states is known as ''open-close'' iteration (Shi, 1988).

For each point-to-face contact, there are three possible states: open, sliding and locked. At an open contact, no springs or frictional forces are applied. At a sliding contact, a normal spring and a pair of frictional forces are applied. At a locked contact, a normal spring and a shear spring are applied. Within a time step, iterations are required to obtain a set of converged contact conditions for the block system, and the state of a contact may change from iteration to iteration. For the open-close iteration algorithm developed for 3D DDA, the criteria for changing from one contact state before an iteration to another state after an iteration are given in Table 1. Once the contact state is determined after an iteration, operations given in Table 2 are performed for different changes in the contact state. Through these operations the open-close iteration should eventually give a set of converged contact conditions for a given block system, with no large penetrations at closed contacts and no tensions in

Table 1. Criteria for contact state changes

Before iteration \ After iteration	Open	Sliding	Locked
Open	$d_n > 0$	$d_n < 0$ and $p_s\|d_s\| > p_n\|d_n\| \tan\phi$	$d_n < 0$ and $p_s\|d_s\| \le p_n\|d_n\| \tan\phi$
Sliding	$d_n > 0$	$d_n < 0$ and $\vec{F} \cdot \vec{L} < 0$	$d_n < 0$ and $\vec{F} \cdot \vec{L} \ge 0$
Locked	$d_n > 0$	$d_n < 0$ and $p_s\|d_s\| > p_n\|d_n\| \tan\phi$	$d_n < 0$ and $p_s\|d_s\| \le p_n\|d_n\| \tan\phi$

Notes:
1. d_n is the normal penetration distance calculated after the iteration; $d_n > 0$ indicates an open contact.
2. d_s is the displacement of the contact point parallel to the contact face calculated after the iteration.
3. p_n is the normal spring stiffness, and p_s is the shear spring stiffness.
4. ϕ is the friction angle.
5. $\vec{L}$ is the projection of $\overrightarrow{P_0'P_1'}$ on the contact face determined after the iteration (see Fig. 2).
6. $\vec{F}$ is the frictional force vector acting at the contact point P_1 (see Fig. 2), determined after the previous iteration.

Table 2. Operations for different contact state changes

Before iteration \ After iteration	Open	Sliding	Locked
Open	none	add normal spring and frictional forces	add normal and shear springs
Sliding	remove normal spring and frictional forces	none	add shear spring and remove frictional forces
Locked	remove normal and shear springs	remove shear spring and add frictional forces	none

normal springs. Convergence is reached when each of the contact states and sliding directions remains the same after an iteration, within set tolerances.

As an illustrative test of the open-close iteration algorithm developed for 3D DDA, a three-block system as shown in Fig. 3a is considered. All three blocks are cubes, with the fixed bottom block having dimensions of $5\,\text{m} \times 5\,\text{m} \times 5\,\text{m}$ and the top two blocks having dimensions of $2\,\text{m} \times 2\,\text{m} \times 2\,\text{m}$. The middle block is subjected to two horizontal forces F_1 and F_2. F_1 acts in the positive x-direction at the centre of a face parallel to the $y-z$ plane, and F_2 acts in the positive y-direction at the centre of a face parallel to the $x-z$ plane. The material constants for the three blocks are: Young's modulus $E = 10\,\text{MPa}$, Poisson's ratio $\nu = 0.3$, and unit weight $\gamma = 14\,\text{kN/m}^3$. The interface properties are: friction angle $\phi = 30^\circ$, cohesion $c = 0$, normal spring stiffness $p_n = 500\,\text{kN/mm}$, and shear spring stiffness $p_s = 200\,\text{kN/mm}$. Two different analyses are carried out with different magnitudes of the two horizontal forces F_1 and F_2. For each analysis, the 2 face-to-face contacts between the blocks are converted to 8 point-to-face contacts as shown in Fig. 3a, and the initial contact states of all point-to-face contacts are assumed to be locked. When $F_1 = F_2 = 20\,\text{kN}$, the top two blocks

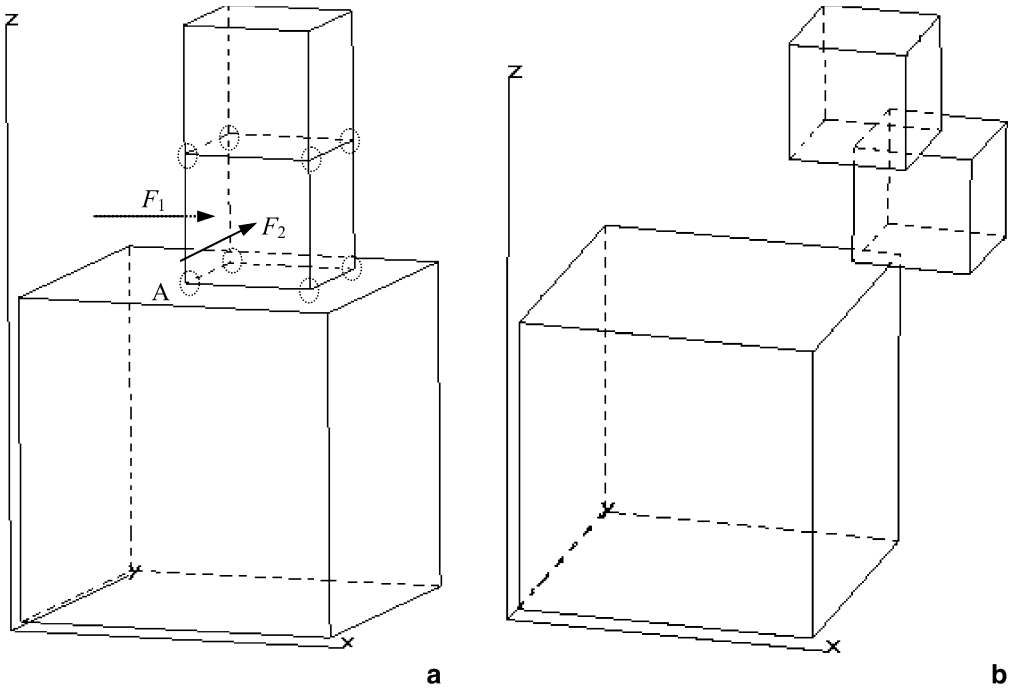

Fig. 3. a Initial configuration of three-block system. **b** Configuration of three-block system after 400 time steps. ○ Point-to-face contact

are stationary. After one iteration within the first time step, the states of all 8 point-to-face contacts remain locked and therefore convergence is reached. When $F_1 = F_2 = 200\,\text{kN}$, although the same initial contact states are assumed, all the contact states converge to sliding after 5 iterations within the first time step. Table 3 gives details of the iterations within the first time step for the point-to-face contact A shown in Fig. 3a. It shows how the criteria in Table 1 and operations in Table 2 are used to

Table 3. Open-close iterations for point-to-face contact A within the first time step

Iteration	d_n (mm)	d_s (mm)	F (kN)	$\vec{L}$	Contact state before iteration	Contact state after iteration
1	−0.00286	0.441	0	[0.311 0.312 0]	locked	sliding
2	−0.03004	12.845	0.83	[9.068 9.096 0]	sliding	sliding
3	0.02003	7.432	8.67	[5.277 5.233 0]	sliding	open
4	−0.07000	11.387	0	[8.046 8.058 0]	open	sliding
5	−0.00667	9.767	20.2	[6.916 6.896 0]	sliding	sliding

Notes:
1. d_n is the normal penetration distance calculated after the iteration; $d_n > 0$ indicates an open contact.
2. d_s is the displacement of the contact point parallel to the contact face calculated after the iteration.
3. The normal spring stiffness, p_n, is $500\,\text{kN/mm}$; and the shear spring stiffness, p_s, is $200\,\text{kN/mm}$.
4. $\vec{L}$ is the projection of $\overrightarrow{P_0'P_1'}$ on the contact face determined after the iteration (see Fig. 2).
5. F is the frictional force magnitude calculated from the normal penetration distance obtained after the previous iteration.

arrive at the converged contact state and sliding direction for this particular point-to-face contact. Figure 3b shows the configuration of the three-block system after some relative sliding of the blocks at the end of time step 400.

The efficiency of the open-close iteration algorithm is demonstrated by some test cases given in the next section. In each of these cases, usually fewer than several iterations are required to obtain convergence of the solution within a time step. As the solution is obtained by simply adding contact submatrices to the global stiffness and force matrices or subtracting contact submatrices from them, the number of equations is not increased, leading to high efficiency in solving the equilibrium equations.

4. Test Cases

The point-to-face contact model is implemented into a 3D DDA program. To validate the model, five test cases are solved using the program and the solutions in two cases compared with analytical solutions.

4.1 Case 1: Block Sliding on Inclined Plane

As shown in Fig. 4a, this case involves a single block sliding down an inclined plane. When the friction angle ϕ is less than the slope angle α, the block accelerates down the slope. For a block initially at rest under the acceleration due to gravity g, the analytical solution for its displacement S as a function of time t is given by:

$$S = \frac{1}{2}at^2 = \frac{1}{2}(g\sin\alpha - g\cos\alpha\tan\phi)t^2. \tag{54}$$

Figure 4b shows the results computed by 3D DDA at the end of 100 time steps. Figure 4c shows the plots of the analytical solutions compared to the 3D DDA results for a plane inclined at 33°, for three different values of the friction angle ϕ of 0, 10° and 20°. This figure shows that the analytical solutions agree well with the results computed by 3D DDA.

4.2 Case 2: Wedge Failure

As shown in Fig. 5a, this case involves a symmetrical wedge sliding on two intersecting frictionless planes. Let α be the dip of the line of intersection of the two planes. The sliding distance S along the intersection line as a function of time t is given by:

$$S = \frac{1}{2}g\sin\alpha\, t^2. \tag{55}$$

Figure 5b shows the results computed by 3D DDA at the end of time step 50 for $\alpha = 60°$. Figure 5c shows the plots of the analytical solutions and 3D DDA results for three different values of the dip angle α of 30°, 45° and 60°. This figure shows that the 3D DDA results agree well with the analytical solutions.

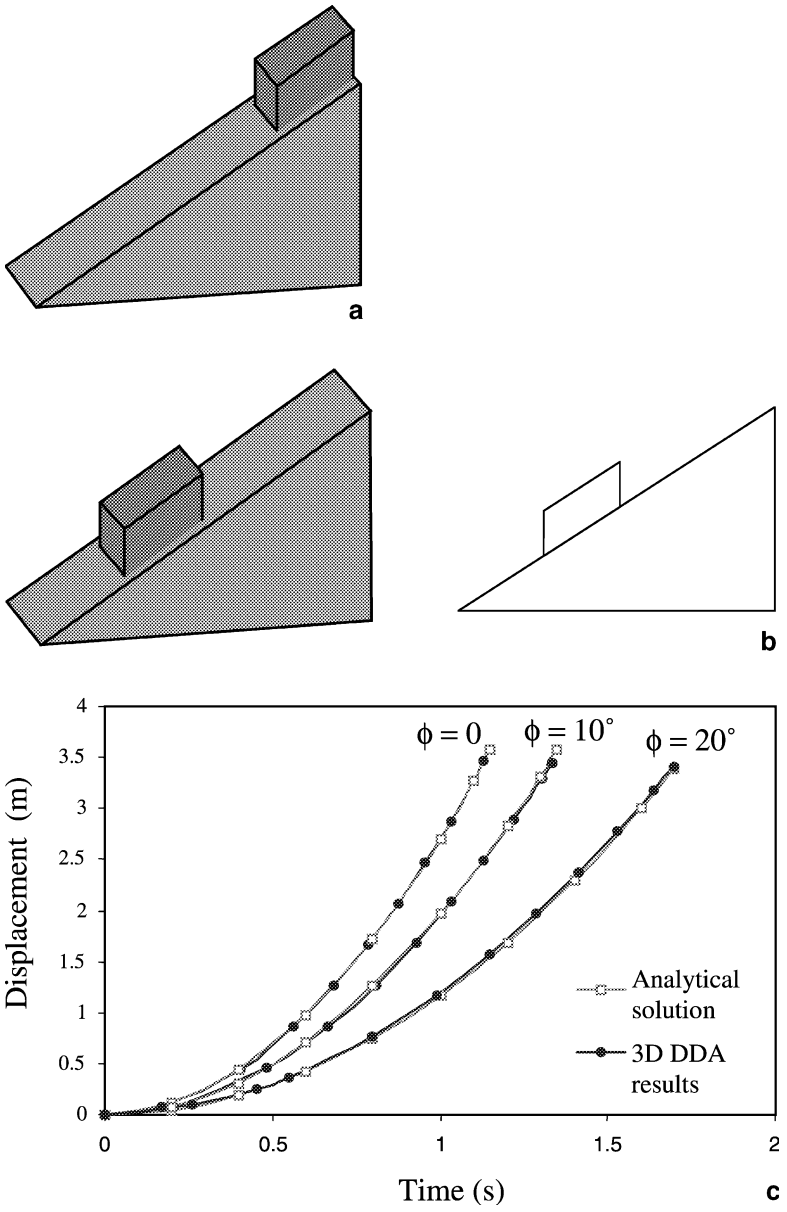

Fig. 4a–c. Case 1: **a** Block sliding on inclined plane; **b** 3D DDA results; **c** comparison between 3D DDA results and analytical solutions

Consider another symmetrical wedge resting on two intersecting planes, each having a friction angle of 20° and with the intersection line dipping at 30°, as shown in Fig. 6a. Fig. 6b shows the results computed by 3D DDA at the end of time steps 50 and 120. As shown in this figure, after the wedge has slid for a certain distance,

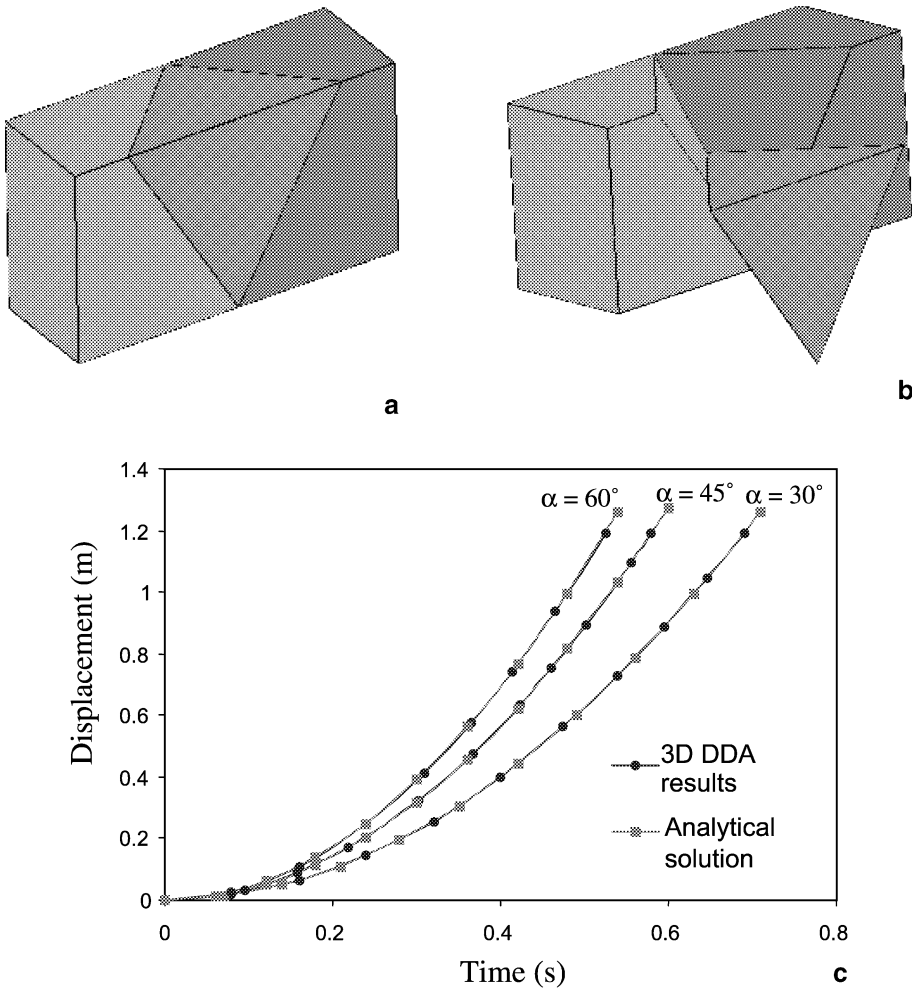

Fig. 5a–c. Case 2: **a** Wedge failure (on frictionless planes); **b** 3D DDA results; **c** comparison between 3D DDA results and analytical solutions

toppling of the block occurs. This case shows that the implemented point-to-face contact model for 3D DDA can handle general modes of wedge failure including simultaneous sliding and rotation.

4.3 Case 3: Rock Fall

As shown in Fig. 7a, this case involves a rock fall in which both angular acceleration and rigid block rotation are considered. The slope angle and friction angle are 45° and 35° respectively. The block falls freely initially and then bounces down the slope. Figure 7b shows the trajectory of the block computed by 3D DDA. It can also be seen

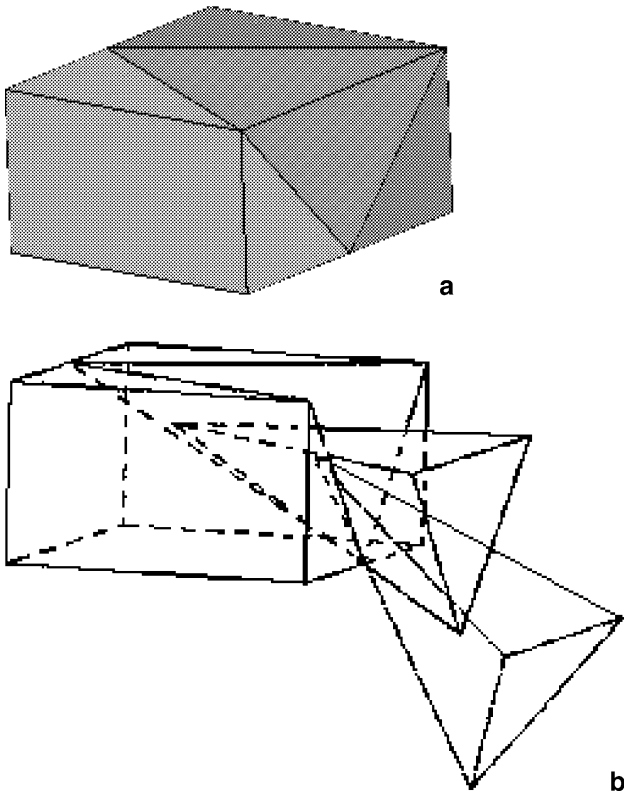

Fig. 6a, b. Case 2: **a** Wedge failure (friction angle = 20°); **b** 3D DDA results showing simultaneous sliding and rotation

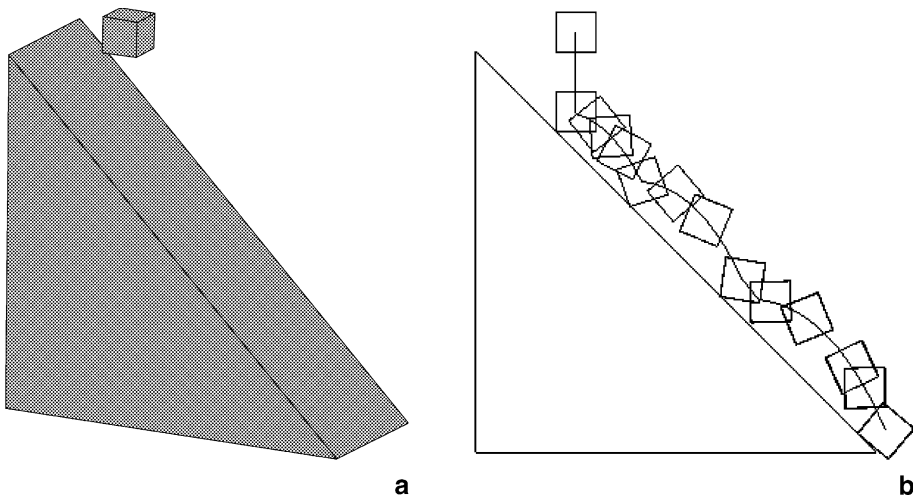

Fig. 7a, b. Case 3: **a** Rock fall; **b** trajectory of block computed by 3D DDA

from this figure that the use of the linear displacement function with post-correction effectively eliminates the block expansion due to rigid body rotation.

4.4 Case 4: Underground Opening

As shown in Fig. 8a, a model of an underground opening consisting of rock blocks is subjected only to the self-weights of the blocks. The boundary conditions are that the boundaries perpendicular to the y- and z-axes ($y = 0$, 5 m and $z = 0$, 5 m) are fixed, and the boundaries perpendicular to the x-axis ($x = 0$, 6 m) are free. The material constants for all the blocks are: Young's modulus $E = 2$ MPa, Poisson's ratio $\nu = 0.25$, friction angle $\phi = 30^\circ$ and cohesion $c = 0$. Fig. 8b shows the large movements computed by 3D DDA of unstable blocks above the roof and in the sidewalls of the opening.

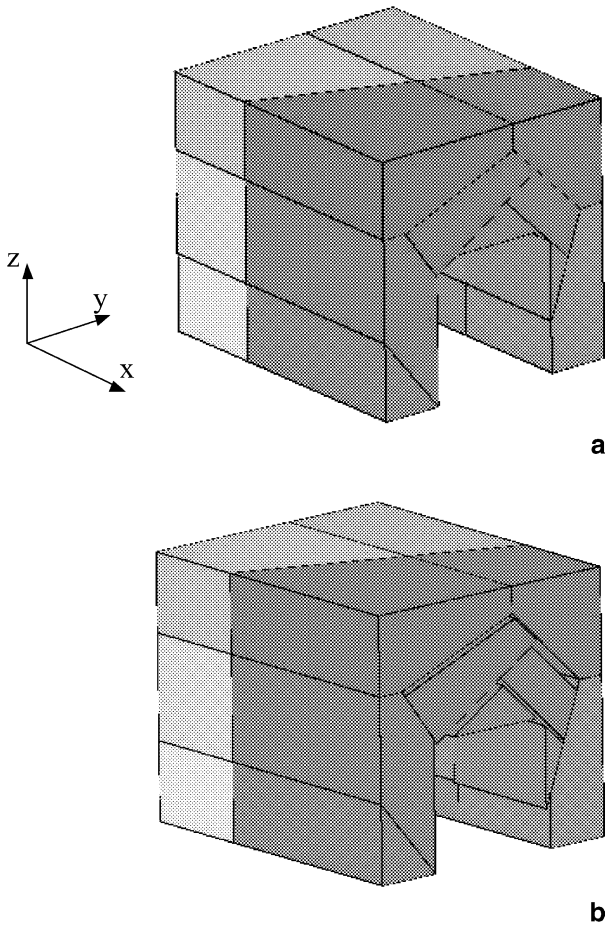

Fig. 8a, b. Case 4: **a** Underground opening; **b** 3D DDA results

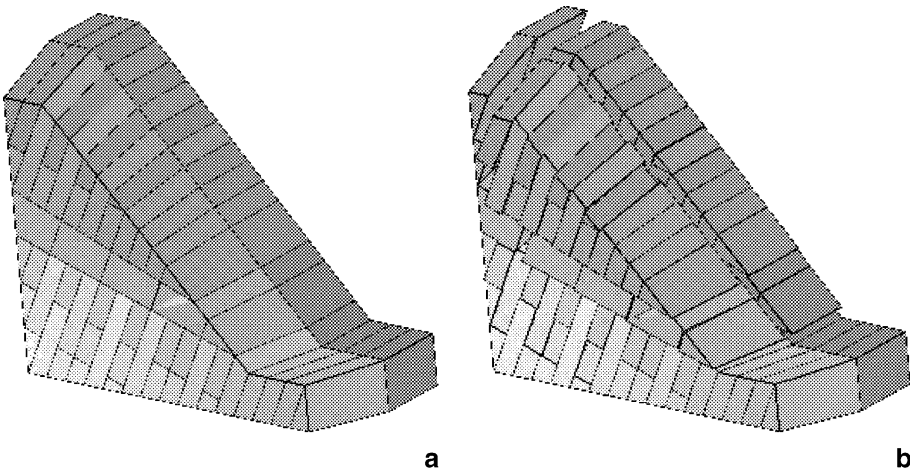

Fig. 9a, b. Case 5: **a** Jointed rock slope; **b** 3D DDA results

4.5 Case 5: Jointed Rock Slope

As shown in Fig. 9a, this case involves a jointed rock slope consisting of 100 blocks. The bottom boundary and the boundary behind the slope are fixed in their respective normal directions, and the other boundaries are free. The material constants for all the blocks are: Young's modulus $E = 170\,\text{MPa}$, Poisson's ratio $\nu = 0.25$, friction angle $\phi = 15^\circ$ and cohesion $c = 0$. The blocks are acted on by their self-weights only. Figure 9b shows the results computed by 3D DDA at the end of time step 100. The progressive failure and discontinuous deformations of the slope, such as the opening of block interfaces and the sliding of blocks, can be clearly seen from the output graphics. It would be difficult to simulate this deformation mode by conventional FEM or other continuum-based numerical methods. This test case demonstrates the effectiveness and capability of the proposed model for complicated problems involving jointed rocks.

5. Conclusions

Discontinuous rock mass behaviour is highly directional in nature and is therefore controlled mainly by the orientations of the discontinuities in the rock mass. As a result, 2D analysis of most practical engineering problems involving discontinuous rocks can only be approximate. For these problems, 3D, instead of 2D, DDA would be more appropriate. This paper describes the basic principles of 3D DDA. As in 2D DDA, a linear displacement function is used implying constant stresses and strains throughout a block, and the equilibrium equations are established by minimizing the total potential energy.

A contact theory governing the discontinuous contacts between arbitrarily shaped polyhedral blocks is an important part of 3D DDA. In this paper, a point-to-face contact model, which forms a part of the contact theory, is presented, and the related contact formulas, including those for the normal spring, shear spring and the frictional

force submatrices are derived in detail, using vector analysis and the penalty method. It can be seen that the contact submatrices are relatively simple and can readily be implemented into a computer code. The number of governing equations is not increased because of the contacts, and the solution can be obtained simply by adding contact submatrices to the stiffness and force matrices or by subtracting contact submatrices from them. Also given is the open-close iteration algorithm developed for 3D DDA, including the open-close iteration criteria and operations performed for different changes in contact state. This algorithm is shown to be efficient.

Five test cases are given to show the validity of the point-to-face contact model. In all 5 cases, the 3D DDA results obtained are reasonable. In 2 cases, the 3D DDA results agree well with analytical solutions.

Acknowledgements

The work reported in this paper has received financial support from the Department of Civil Engineering, University Research Committee, and the Committee on Research and Conference Grants, all of The University of Hong Kong, and from the Natural Science Foundation of China (50239070). This support is gratefully acknowledged.

References

Bathe, K. J., Chaudhary, A. (1985): A solution method for planar and axisymmetric contact problems. Int. J. Numer. Meth. Engng. 21, 65–88.

Chaudhary, A., Bathe, K. J. (1986): A solution method for static and dynamic analysis of three-dimensional contact problems with friction. Comput. Struct. 24, 855–873.

Chen, G. Q., Miki, S., Ohnishi, Y. (1997): Development of the interactive visualization system for DDA. In: Proc., 9th Int. Conf. on Computer Methods and Advances in Geomechanics, Wuhan, China, 495–500.

Chen, H. W., Tsai, P. (1986): Finite element analysis of elastodynamics sliding contact problems with friction. Comput. Struct. 22, 925–938.

Chern, J. C., Koo, C. Y., Chen, S. (1990): Development of second order displacement function for DDA and manifold method. Working forum on the manifold method of material analysis, Vicksburg, 183–202.

Cundall, P. A. (1988): Formulation of a three-dimensional distinct element model - part I: a scheme to detect and represent contacts in a system composed of many polyhedral blocks. Int. J. Rock Mech. Min. Sci. Geomech. Abstr. 25, 107–116.

Fischer, U., Melosh, R. J. (1987): Solving discretized contact problems using linear programming. Comput. Struct. 25, 661–664.

Francavilla, A., Zienkiewicz, O. C. (1975): A note on numerical computational of elastic contact problems. Int. J. Numer Meth. Engng. 9, 913–924.

Hatzor, Y. H., Feintuch, A. (2001): The validity of dynamic block displacement prediction using DDA. Int. J. Rock Mech. Min. Sci. 38, 599–606.

Hong, X., Shen, G. X., Kihara, J., Aizawa, T. (1998): Three-dimensional elasto-plastic contact boundary element method with friction. Chin. J. Comput. Mech. 15, 32–37.

Jing, L. R., Ma, Y., Fang, Z. L. (2001): Modeling of fluid flow and solid deformation for fractured rocks with discontinuous deformation analysis (DDA) method. Int. J. Rock Mech. Min. Sci. 38, 343–355.

Kanto, Y., Yagawa, G. (1990): A dynamic contact buckling analysis by the penalty finite element method. Int. J. Numer. Meth. Engng. 29, 755–774.

Ke, T. C. (1996): The issue of rigid-body rotation in DDA. In: Proc., First International Forum on Discontinuous Deformation Analysis (DDA) and Simulations of Discontinuous Media, Berkeley, U. S. A., 318–325.

Kim, Y. I., Amadei, B., Pan, E. (1999): Modeling the effect of water, excavation sequence and rock reinforcement with discontinuous deformation analysis. Int. J. Rock Mech. Min. Sci. 36, 949–970.

Klarbring, A. (1986): A mathematical programming approach to three-dimensional contact problems with friction. Comput. Methods Appl. Mech. Engng. 58, 175–200.

Koo, C. Y., Chern, J. C. (1998): Modification of the DDA method for rigid block problems. Int. J. Rock Mech. Min. Sci. 35, 683–693.

Leung, A. Y. T., Chen, G. Q., Chen, W. J. (1998): Smoothing Newton method for solving two- and three-dimensional frictional contact problems. Int. J. Numer. Meth. Engng. 41, 1001–1027.

Lin, C. T., Amadei, B., Jung, J., Dwyer, J. (1996): Extensions of discontinuous deformation analysis for jointed rock masses. Int. J. Rock Mech. Min. Sci. 33, 671–694.

Li, X. W., Soh, A. K., Chen, W. J. (2000): A new non-smooth model for three dimensional frictional contact problems. Comput. Mech. 26, 528–535.

Munjiza, A., Andrews, K. R. F. (2000): Penalty function method for combined finite-discrete element systems comprising large number of separate bodies. Int. J. Numer. Meth. Engng. 49, 1377–1396.

Oden, J. T., Kikuchi, N. (1982): Finite element methods for constrained problems in elasticity. Int. J. Numer. Meth. Engng. 18, 701–725.

Rahman, M. U., Rowlands, R. E., Cook, R. D. (1984): An iterative procedure for finite element stress analysis of frictional contact problems. Comput. Struct. 18, 947–954.

Shi, G. H. (1988): Discontinuous deformation analysis-a new numerical model for the statics and dynamics of block system. Ph. D. Thesis, Dept. of Civil Engineering, University of California, Berkeley.

Shi, G. H. (2001): Theory and examples of three dimensional discontinuous deformation analyses. In: Proc., 2nd Asian Rock Mechanics Symposium, Beijing, China, 27–32.

Shi, G. H., Goodman, R. E. (1989): Generalization of two-dimensional discontinuous deformation analysis for forward modelling. Int. J. Numer. Anal. Methods Geomech. 13, 359–380.

Sitar, N., MacLaughlin, M. M. (1997): Kinematics and discontinuous deformation analysis of landslide movement. Invited Keynote Lecture II, Pan American Symposium on Landslides, Rio de Janeiro, 10–14.

Thomas, P. A., Bray, J. D. (1999): Capturing nonspherical shape of granular media with disk clusters. ASCE J. Geotechn. Geoenvironm. Engng. 125, 169–178.

Yamazaki, K., Sakamoto, J., Takumi, S. (1994): Penalty method for three-dimensional elastic contact problems by boundary element method. Comput. Struct. 52, 895–903.

Yeung, M. R. (1993): Analysis of a mine roof using the DDA method. Int. J. Rock Mech. Min. Sci. Geomech. Abstr. 30, 1411–1417.

Authors' address: Dr. Man-chu Ronald Yeung, Department of Civil Engineering, The University of Hong Kong, Pokfulam Road, Hong Kong, China; e-mail: mryeung@hku.hk